Novel ZnO/Zn–Cr hydrotalcite-like anionic clay as a high-performance and recyclable material for efficient photocatalytic removal of organic dye under simulated solar irradiation

H.-Y. Zhu[1,2,3] · R. Jiang[1,2] · J. Yao[1,2] ·
F.-Q. Fu[1] · J.-B. Li[3]

Abstract Reusable ZnO/Zn–Cr hydrotalcite-like anionic clays (ZnO/Zn–Cr HACs) were synthesized by a co-precipitation method and characterized by powder X-ray diffraction, Fourier transform infrared spectroscopy, N_2 adsorption–desorption analysis, elemental mapping patterns, scanning electronic microscope, and UV–Vis diffuse reflectance spectra. Its adsorption and photocatalytic activity towards organic pollutant (congo red as a model pollutant) were evaluated. The Langmuir isotherm was used to fit the equilibrium experiments. Saturated adsorption capacity of ZnO/Zn–Cr HACs was 426.29 mg g^{-1} at 308 K. The model pollutant exhibited fast and highly efficient removal from aqueous solution by ZnO/Zn–Cr HACs under simulated solar light irradiation. The experiments of cycles demonstrated that there was no evident change in the removal efficiency of Congo red (CR) solution by ZnO/Zn–Cr HACs the fifth time under simulated solar light irradiation, which indicates that ZnO/Zn–Cr HACs can be reused and will be favorable for effective elimination of toxic organic compounds in wastewater. Therefore, it is expected that ZnO/Zn–Cr HACs with layered structures and high surface areas can be potentially used as effective and reusable materials for large-scale environmental purification.

✉ R. Jiang
  jiangru@tzc.edu.cn; jiangru0576@163.com

✉ J.-B. Li
  jianbing.li@unbc.ca

[1]   Zhejiang Provincial Key Laboratory of Plant Evolutionary Ecology and Conservation, Taizhou University, Taizhou 318000, People's Republic of China

[2]   Department of Environmental Engineering, Taizhou University, Taizhou 318000, People's Republic of China

[3]   Environmental Engineering Program, University of Northern British Columbia, 3333 University Way, Prince George, BC V2N 4Z9, Canada

Introduction

In recent years, there has been an increasing demand for solutions to multiple environmental problems associated with the use of toxic organic compounds [1–3]. Amongst toxic organic compounds, organic dyes represent an important class of environmental pollutant found in the effluent from various industries, such as printing, textile, dyeing, paper, leather, tannery, and paint industries. [4]. Generally, those dyes are harmful to flora and fauna, and some of the dyes have been reported to be carcinogenic and mutagenic [5]. However, most of those dyes have a complex molecular structure and are stable and difficult to be treated by conventional biological methods [6, 7]. Therefore, effective removal of organic dye pollutants from wastewater before discharge is necessary in order to reduce their negative effect on both the aqueous environment and human health [8]. In recent years, there has been increasing interest in developing feasible methods for treatment of dye-containing wastewater [9–13]. Among these approaches, adsorption and photocatalytic removal of organic dye pollutant from aqueous solution have been shown to be an effective technique [5, 14–16].

Hydrotalcite-like anionic clays (HACs), also known as layered double hydroxides (LDHs) materials, are rare in nature but can be synthesized readily. As anionic clays, HACs are generally expressed as $\left[M_{1-x}^{2+}M_x^{3+}(OH)_2\right]^{x+}(A^{n-})_{x/n}\cdot mH_2O$, where M^{2+} represents divalent metal cation, M^{3+} is trivalent metal cation and A^{n-} is an anion [17–20]. Because of their unique layered structure, simplicity of synthesis and high anion exchange capacities, HACs have been attracting considerable attention as environmentally friendly materials for effective removal of pollutants such as phosphates [21, 22], dye [23–25], and oxyanions [26]. HACs adsorb anionic pollutants from aqueous solution via two mechanisms: (1) adsorption and (2) intercalation by anion exchange [26, 27]. Generally, HACs can be reused by the reconstruction of calcined-LDHs in organic anion solutions. However, the fact that inconvenient reconstruction and regeneration of HACs need high temperature restricted greatly their actual application in removal of organic pollutants from practical solutions. Although there are some publications on preparations of Zn–Cr HACs [28], to our knowledge, there is no detailed report so far about adsorption and photocatalytic synergistic removal of organic dye from aqueous solution by reusable (s)-303.6rradi1(appliexchan)-9.8.0037(x-)]TJ-1.13810002 -1.200700T0000610(aim99961(al)-48

congo red and temperature. The maximum adsorption capacity was determined from the Langmuir isotherm. Their photocatalytic performances for photocatalytic decolorization of CR solution by ZnO/Zn–Cr HACs were also investigated under simulated solar irradiation. These results will be useful for further application of ZnO/Zn–Cr HACs in the effective treatment of practical wastewater.

Experimental

Chemicals

Titanium dioxide (P25) with purity of at least 99.5 % was obtained from Degussa. Congo red ($C_{32}H_{22}N_6O_6S_2Na_2$, molecular weight 696.67) used as a model dye was purchased from Yongjia Fine Chemical Factory (Wenzhou, China). $CrCl_3·6H_2O$, $ZnCl_2·7H_2O$, NaOH, Na_2CO_3, and other reagents of analytical grade were purchased from Shanghai Chemical Reagents Research Institute (Shanghai, China). All reagents were used as received without further treatment.

Preparation of ZnO/Zn–Cr HACs

ZnO/Zn–Cr HACs were prepared by a co-precipitation method. Typically, a salt mixture solution (250 mL) containing 0.10 mol of $CrCl_3$ and 0.20 mol of $ZnCl_2$ were added to an alkaline solution (250 mL) containing 1.0 mol of NaOH and 0.33 mol of Na_2CO_3 under vigorous stirring at 65 °C. The pH of mixture was held constant at 12–13. The resulting precipitate obtained was aged with hydrothermal treatment at 65 °C for 18 h. The slurry was collected and washed with distilled water via centrifugation. Finally, the obtained gelatinous precipitate was dried at 80 °C overnight. ZnO was prepared using the same procedure, but without the addition of $CrCl_3$.

Characterization of ZnO/Zn–Cr HACs

N_2 adsorption–desorption isotherms of ZnO/Zn–Cr HACs at 77 K was measured on a Micromeritics ASAP2020, from which the Brunauer–Emmett–Teller (BET) surface area (S_{BET}) and Barrett–Joyner–Halenda (BJH) pore size (d_p) were calculated, respectively. ZnO/Zn–Cr HACs were mounted using a double-sided adhesive tape and coated with gold. The coated samples were observed using a Hitachi SX-650 scanning electron microscope at required magnification. Powder X-ray diffraction (XRD) measurements were performed in a Bruker Advance D8 X-ray diffractometer. Voltage and current used were 40 kV and 30 mA, respectively, and XRD patterns were obtained in the 2θ range of 10°–70° at a 5 ° min^{-1} scan speed. FT-IR spectra were measured at room temperature on a FT-IR-8400 spectrometer (Shimadzu, Japan). UV–Vis diffuse reflectance spectra (DRS) were recorded at room temperature in air on a Shimadzu UV-2501PC spectrometer equipped with an integrating sphere attachment using $BaSO_4$ as a background.

Batch adsorption studies

Adsorption experiments were carried out on a model KYC-1102 C thermostate shaker (Ningbo, China). For a typical batch experiment, about 50 mg of ZnO/Zn–Cr HACs were added into 50 mL of CR solution for 3 h. At predetermined time intervals, 5 mL of dispersion were withdrawn and filtered. Residual CR concentration in the supernate was analyzed at $\lambda_{max} = 496.0$ nm using a TU 1810 model UV–visible spectrophotometer (Purkinje General Co. Ltd, China). Adsorbed amount (q_t) of CR per unit weight of dry ZnO/Zn–Cr HACs at time t and removal efficiency (η) of CR on ZnO/Zn–Cr HACs were calculated by Eqs. (1) and (2), respectively.

$$q_t = \frac{(C_0 - C_t)V}{W} \tag{1}$$

$$\eta(\%) = \frac{(C_0 - C_t)}{C_0} \times 100 \tag{2}$$

where C_0 and C_t (mg L^{-1}) are the initial CR concentration and the CR concentrations at any time t (min), respectively; V (L) is the volume of the CR solution; and m (g) is the weight of ZnO/Zn–Cr HACs used.
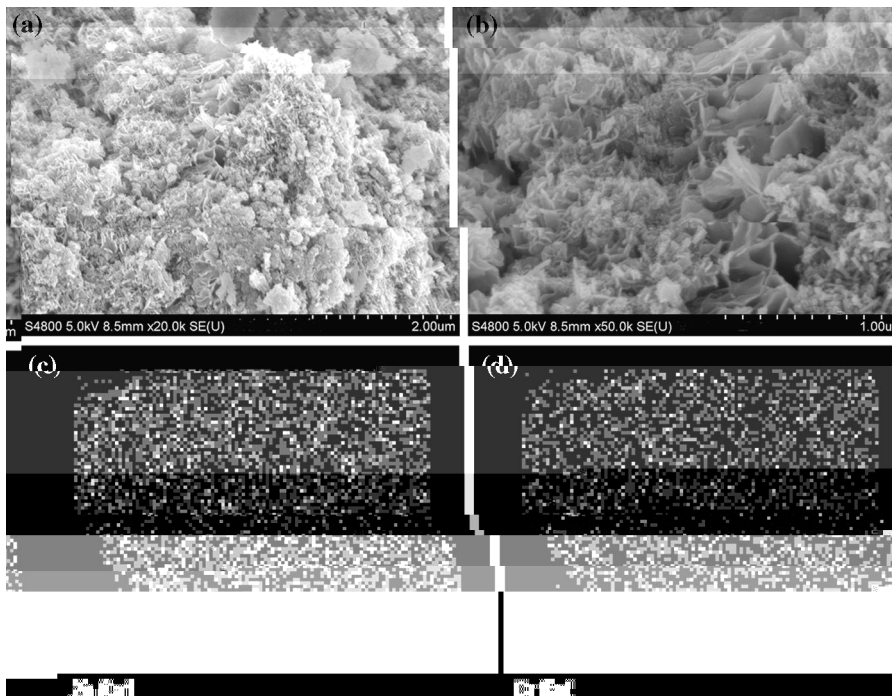

Fig. 1 Typical SEM (a, b) and elemental mapping patterns (c, d) of ZnO/Zn–Cr HACs

Photocatalytic experiments

A 300 W Xenon lamp (PLS-SXE300, Beijing Trust Tech Co. Ltd, China) was used as a simulated solar light source. The wavelength of simulated solar light irradiation was in a range from 300 to 1100 nm. According to a technical report of PLS-SXE300, UV output (<390 nm) was about 5.2 % of irradiation energy while simulated solar light output (390–770 nm) was about 39.2 %. A 50 mL of CR aqueous solution (30 mg L^{-1}) and 50 mg of ZnO/Zn–Cr HACs were added into photocatalytic reactor. During reaction, the resulting aqueous suspension containing CR and ZnO/Zn–Cr HACs was continuously stirred and bubbled so that concentration of dissolved oxygen in reaction system was kept constant. At completion of predetermined time intervals, samples for analyses (about 5 mL) were taken and the filtrates were analyzed on a TU 1810 model UV–visible spectrophotometer (Purkinje General Co. Ltd, China) at $\lambda_{max} = 496.0$ nm for CR solution.

Results and discussion

Characterization of ZnO/Zn–Cr HACs

The characterization of the as-prepared ZnO/Zn–Cr HACs is illustrated in Fig. 1. The synthesized ZnO/Zn–Cr HACs show obvious layered structure and clearly exhibit the presence of hierarchical structure consisting of two-dimensional thin nanoflakes in lateral dimension and 80–120 nm in thickness (Fig. 1a, b). Local elemental mapping has been conducted by energy dispersive X-ray spectroscopy (EDS) to address composition distribution on the ZnO/Zn–Cr HACs. Elemental mappings of Zn and Cr show that Zn and Cr are uniformly distributed on the surface of ZnO/Zn–Cr HACs (Fig. 1c, d). Elemental analysis from EDAX indicates that Zn–Cr atomic ratio is about 2.02.

X-ray diffraction patterns of ZnO/Zn–Cr HACs and pure ZnO are displayed in Fig. 2. Some important peaks located at (0 0 3), (0 0 6), (0 1 2), and (1 1 0) are ascribed to the characteristic peaks of layered double hydroxides(JCPDS 41-1428),

Fig. 2 X-ray diffraction patterns of ZnO/Zn–Cr HACs and ZnO
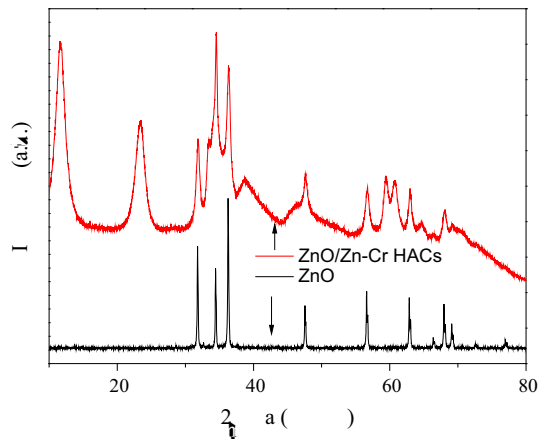
which indicates that the prepared ZnO/Zn–Cr HACs are hydrotalcite-like structure and have typical anion structure [28]. At the same time, in XRD pattern of ZnO/Zn–Cr HACs, other peaks located at (1 0 0), (1 0 1), (1 0 2), and (1 1 2) in Fig. 2 can be indexed as the hexagonal wurtzite structure for ZnO (JCPDS 36-1451) [29–31]. This is because Zn^{2+} undergoes partly hydrolysis at high pH to precipitate ZnO in alkaline condition [32]. No characteristic peaks of other materials were detected, so it can be believed that the prepared materials are a composite of ZnO and Zn–Cr HACs. Generally, coupling of different semiconductor can enhance photocatalytic response to visible light and increase charge separation, resulting in the increase of photocatalytic decolorization of dye wastewater under simulated solar light irradiation [16, 33]. Therefore, ZnO/Zn–Cr HACs were expected to exhibit effective photocatalytic decolorization performance towards dyes.

Figure 3 shows the UV–Vis absorption spectra of ZnO/Zn–Cr HACs and reference sample TiO_2 (P25) using UV–Vis diffuse reflectance spectra (UV–Vis DRS). Obviously, P25 only showed absorption edge about 400 nm, which is in agreement with the literature [34]. As expected, ZnO/Zn–Cr HACs exhibit enhanced absorption in the visible light region (400–700 nm). As observed from UV–Vis DRS of ZnO/Zn–Cr HACs composites (Fig. 1d), ZnO/Zn–Cr HACs composites were characterized by two main bands in the visible region with maximum absorption at 564.3 and 412.2 nm. According to reported literature, the enhancement of photocatalytic activity was explained on the basis of electronic structure of LDH, where Cr^{3+} played an indispensable role [25]. In addition, the photodegradation of anionic dyes was accelerated by their own photosensitization action on the LDH layer. A possible reaction pathway is that the dye molecules adsorbed on LDH surface is first excited under light irradiation.

Adsorption of CR onto ZnO/Zn–Cr HACs

The adsorption kinetics is important because they can provide valuable insights into the mechanism of solid/liquid adsorption. Therefore, in order to investigate the kinetics of adsorption of CR onto ZnO/Zn–Cr HACs, two common adsorption
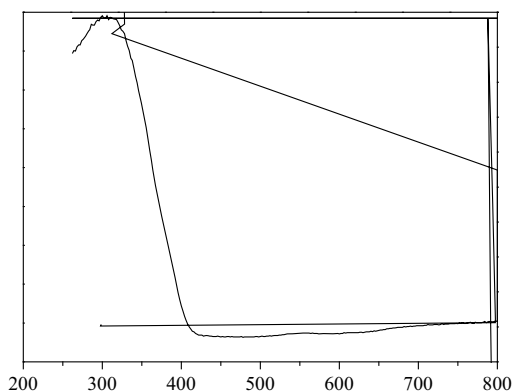
kinetic equations were employed to simulate the procedure, that is, the pseudo-second-order equation (Eq. 3) and intraparticle diffusion model (Eq. 4) as expressed below:

$$\frac{t}{q_t} = \frac{1}{k_2 q_e^2} + \frac{1}{q_e} t \tag{3}$$

$$q_t = k_{id} t^{1/2} + c \tag{4}$$

where q_e and q_t are the amount of CR adsorbed (mg g^{-1}) on the adsorbents at the equilibrium and at time t, respectively; k_2 is the rate constant of pseudo-second-order adsorption (g mg^{-1} min^{-1}). Values of k_2 are obtained from plotting (t/q_t) versus t. c is the intercept (mg g^{-1}). k_{id} is the intraparticle diffusion rate constant, which can be evaluated from the slope of the linear plot of q_t versus $t^{1/2}$.

Figure 5 shows the kinetics of CR adsorption on different initial concentrations for an adsorbent dosage of 1.0 g L^{-1}. The values of R of the pseudo-second-order equation were obtained from the linear plots of t/q_t versus t. The high R values obtained indicate that it was feasible for the applicability of the pseudo-second-order kinetic model to describe the adsorption process of CR on ZnO/Zn–Cr HACs (Fig. 5a). The pseudo-second-order model is based on the assumption that the rate-determining step may be a chemical sorption involving valence forces through exchange or sharing of electrons between sorbate and adsorbent [35]. In fact, a major mechanism when HACs adsorb anionic pollutants from aqueous solution is the intercalation by anion exchange [27]. For a solid–liquid adsorption process, the solute transfer is usually controlled either by particle diffusion or by intraparticle diffusion. At least three independent rate-controlling mechanisms appear to compete with each other and dominate the different stages of adsorption (Fig. 4b) [24]. According to Fig. 4b, the adsorption of CR onto ZnO/Zn–Cr HACs went through three independent rate-controlling stages. Generally, the first stage is attributed to the external surface adsorption correlated to the boundary layer diffusion, which is assumed to occur rapidly and does not form a rate-limiting stage
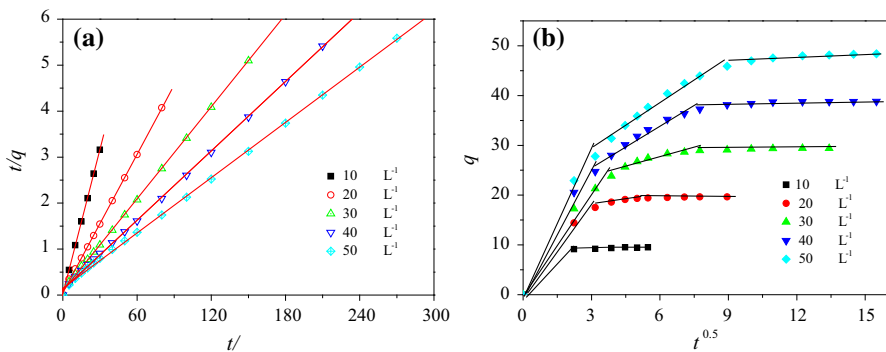

Fig. 4 Plots of the pseudo-second-order model and intraparticle diffusion model at different initial dye concentrations on ZnO/Zn–Cr HACs

in the adsorption of CR on ZnO/Zn–Cr HACs. In fact, the first stage could be completed after about 5 min. With increase in CR concentration, the second stage appeared and was prolonged. All linear dependence for the second stage did not pass through zero, which indicates that intraparticle diffusion is involved in the adsorption process, but is not the only rate-controlling step. The values of intercept give an idea about the boundary layer thickness [36]. The intercept decreased with the increase of the initial CR concentration, which indicates that the greater is the boundary layer effect when the initial concentration of CR is lower.

Adsorption isotherms

The equilibrium adsorption isotherm is essential for describing the interactive behavior between solutes and adsorbent and is important in the design of an adsorption system. In this work, equilibrium data for CR adsorption on ZnO/Zn–Cr HACs were modeled using the Langmuir equation (Eq. 5) and Freundlich equation (Eq. 6).

$$q_e = \frac{q_m K_L C_e}{1 + K_L C_e} \tag{5}$$

$$q_e = K_F C_e^{\frac{1}{n}} \tag{6}$$

where q_m is the maximum amount of adsorption (mg g^{-1}), and K_L is the Langmuir binding constant, which is related to the energy of adsorption (L mg^{-1}). C_e is the concentration of the dye solution at adsorption equilibrium (mg L^{-1}), K_F [mg g^{-1} (L g^{-1})$^{-1/n}$] and n are the Freundlich constants related to the adsorption capacity and intensity, respectively.

The Langmuir adsorption isotherm assumes that adsorption takes place at specific homogeneous sites within the adsorbent, and it has been used successfully for many adsorption processes of monolayer adsorption. The values q_m, K_F, n, and the related correlation coefficients (R^2 values) are summarized in Table 1. Figure 5 shows the fitted equilibrium data in Langmuir and Freundlich models for CR adsorption onto ZnO/Zn–Cr HACs. Obviously, the fact that the Langmuir isotherm fits the experimental data very well may be due to homogeneous distribution of active sites onto ZnO/Zn–Cr HACs (Fig. 5; Table 1). In fact, the elemental mappings of Zn and

Table 1 Freundlich and Langmuir isotherms of ZnO/Zn–Cr HACs

| T (K)	Langmuir isotherm constants				Freundlich isotherm constants		
	$q_{e,exp}$ (mg g^{-1})	$q_{m,cal}$ (mg g^{-1})	K_L (L mg^{-1})	R^2	K_F (mg$^{1-(1/n)}$ L$^{1/n}$ g^{-1})	n	R^2
308	426.29	414.93	0.1111	0.994	47.50	2.84	0.857
318	359.56	358.42	0.1166	0.999	52.00	3.74	0.795
328	293.34	289.85	0.1389	0.998	45.63	3.68	0.714

Cr (Fig. 1c, d) also have proven that Zn and Cr are uniformly distributed on the ZnO/Zn–Cr HACs. The Langmuir model is based on the assumptions that all the adsorption sites are equivalent (i.e. the surface of the adsorbent is uniform), all adsorption occurs by the same mechanism, adsorbed molecules do not interact with one another, and only a monolayer is formed at the maximum adsorption. The equilibrium parameter, K_L values were between 0.11 and 0.14, which indicates favorable conditions for adsorption at all the temperatures studied (Table 1). Also, as seen in Table 1, maximum adsorption capacities for CR onto ZnO/Zn–Cr HACs at 308, 318, and 328 K were found to be 426.29, 359.56, and 293.34 mg g^{-1}, respectively. In addition, with an increase in temperature, the K_L values increase, indicating that CR removal by ZnO/Zn–Cr HACs is an exothermic process [26].

Reuse of ZnO/Zn–Cr HACs under simulated light irradiation

From a practical viewpoint, reusability of ZnO/Zn–Cr HACs must be required to evaluate the stability. After adsorption for 180 min, 96.6, 93.0, 81.5, 79.4, and 67.3 % of CR was decolorized in the first and further use by ZnO/Zn–Cr HACs, respectively (Fig. 6, curve a). Obviously, however, the decolorization percentage of CR solution by ZnO/Zn–Cr HACs for five cycles use were 99.7, 99.3, 98.6, 97.9, and 96.3 % after 180 min of simulated solar irradiation, respectively (Fig. 6, curve b). It was observed that ZnO/Zn–Cr HACs can be used for a fifth time with 96.3 % decolorization efficiency after 180-min treatment by synergy of adsorption and photocatalysis. This result indicates that it will be favorable for the effective elimination of toxic organic compounds in wastewater by using ZnO/Zn–Cr HACs under simulated solar light irradiation. Therefore, it is expected that the ZnO/Zn–Cr HACs with layered structures and high surface areas in this work can be potentially used as an effective and reusable materials for large-scale environmental purification under simulated solar light irradiation.

To demonstrate changes of molecular and structural characteristics of CR by ZnO/Zn–Cr HACs in dark or under simulated solar light irradiation, representative UV–Vis spectra of CR solution were depicted in Fig. 7. As observed from the

Fig. 5 Liquid phase adsorption isotherms of CR on ZnO/Zn–Cr HACs
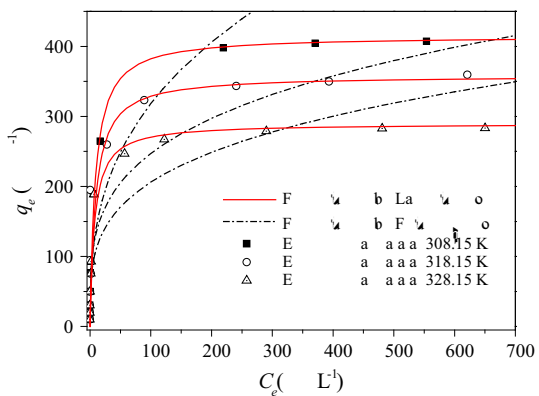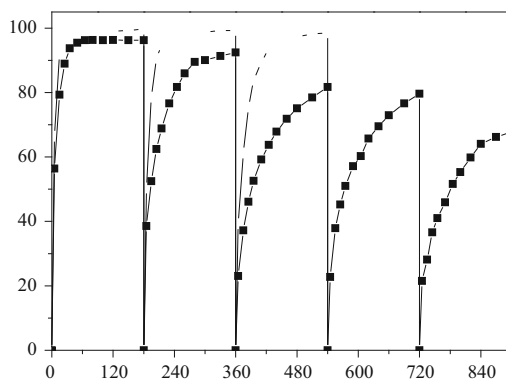
original UV–Vis spectrum (Fig. 7, curve a), CR solution was characterized by one main band in the visible region with maximum absorption at 496 nm and by other two bands in the ultraviolet region at 339.0 and 239 nm [37]. The peak at 239 nm was associated with "benzene-like" structures in the molecule [38]. The peak at 496 nm originated from extended chromospheres that are connected through the azo bond, which resulted in red color in aqueous solution (Inset A in Fig. 7). Figure 7, curve b showed that the absorbance at 496 and 339 nm decreased from 0.906 to 0.267 and from 0.37 to 0.269, respectively, in the presence of the ZnO/Zn–Cr HACs in dark with continuous stirring. At the same time, the locations of both peaks did not change. The CR solution after adsorption by ZnO/Zn–Cr HACs was still a faint red (Inset B in Fig. 7). However, the main band in the visible region disappeared completely and the absorbance at 496 nm decreased to 0.031 while for the adsorption and photocatalysis under simulated solar light irradiation by ZnO/Zn–Cr HACs after treatment for 180 min (Fig. 7, curve c), which indicated that azo linkages of CR were destroyed partly and CR solution was decolorized effectively (Inset C in Fig. 7). The disappearance of the visible band with treatment time was

due to the fragmentation of the azo links by direct ozone attack. In addition to this rapid bleaching effect, the decay of the absorbance at 339 nm was considered as evidence of aromatic fragment degradation in the dye molecule and its intermediates [37].

In order to give a further understanding of adsorption and photocatalytic performance of the ZnO/Zn–Cr HACs, some characterizations were further performed. BET surface areas and pore size distributions of the sample were determined from nitrogen adsorption desorption data measured using Brunauer–Emmett–Teller method and presented in Fig. 8a. All three samples exhibit similar pore size distributions, which indicate that the structure of ZnO/Zn–Cr HACs didn't change after adsorption and photocatalytic activity. However, the BET surface area (S_{BET}) of raw ZnO/Zn–Cr HACs, ZnO/Zn–Cr HACs after irradiation and ZnO/Zn–CrZn–Cr HACs after adsorption were 145.36, 139.57, and 115.68 m^2 g^{-1}, respectively. These results suggest that the CR molecular adsorbed in/on ZnO/Zn–Cr HACs have been removed by photocatalysis under simulated solar irradiation.

FT-IR spectrum of ZnO/Zn–Cr HACs was compared before or after adsorption and photoirradiation. The spectra recorded in the 400–4000 cm^{-1} range for CR, ZnO/Zn–Cr HACs-CR after adsorption, ZnO/Zn–Cr HACs-CR after irradiation and ZnO/Zn–Cr HACs-CR are presented in Fig. 8b. For ZnO/Zn–Cr HACs the broad and strong band centered at 3408 cm^{-1} corresponds to the O–H stretching vibration of hydroxyl groups in the layers and interlayer water molecules and this is attributed to the formation of hydrogen bonding of interlayer water with the different anions as well as with the hydroxide groups of the layers [39]. The bands centered at 1358 cm^{-1} in the spectrum are attributed to the strong interaction of carbonate anions with the layer. The bands appearing at 600–900 cm^{-1} centered at 781 cm^{-1} and the sharp band observed at about 515 cm^{-1} can be attributed to the cation–oxygen (M–O) vibrations [40]. In FTIR spectrum of CR dye (Fig. 8b), 1613 cm^{-1} for the stretching vibrations of aromatic C–C and/or N=N bonds, 1178 and 1057.7 cm^{-1} for the obvious bands of S=O and SO$_3^-$ group, and 1558 cm^{-1} for N–H bend. The adsorption of CR is supported by FT-IR experiments. Compared
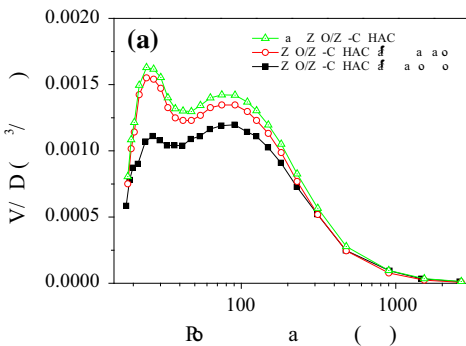
with the FTIR spectra of ZnO/Zn–Cr HACs, the absorption bands of CR are observed in ZnO/Zn–Cr HACs-CR after adsorption, such as 1610 and 1420 cm^{-1} for the stretching vibrations of aromatic C–C and/or N=N bonds, 1177 and 1057 cm^{-1} for the significant bands of S=O and SO^{3-} group, and 1515 cm^{-1} for N–H bend. After adsorption of CR the band observed at 1364 cm^{-1} becomes very strong and sharp and shifts to higher wavenumber (1383 cm^{-1}).
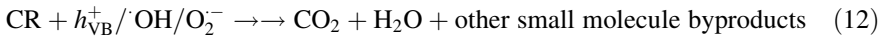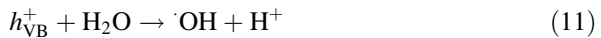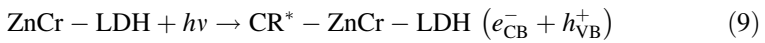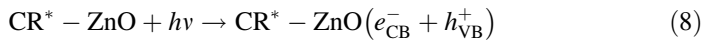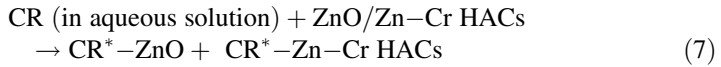
Comparisons of decolorizatin by ZnO, P25, and ZnO/Zn–Cr HACs

For comparison, decolorization experiments were carried out using three different materials (ZnO/Zn–Cr HACs, P25, and ZnO) and the corresponding results are shown in Fig. 9. After 20 min of simulated solar light irradiation, the decolorization percentage of CR solution (30 mg L^{-1}) reached 37.4 and 14.4 % by P25 and ZnO, respectively. However, 92.0 % of CR solution was decolorized in the presence of ZnO/Zn–Cr HACs, which was 54.6 and 77.6 % higher than photocatalysis in the presence of P25 and ZnO, respectively. Before and after treatment of photocatalytic reactions, TOC values of CR solution were measured using a TOC-V CPH Analyzers (Shimadzu, Japan). TOC removal rate of the model wastewater was about 87.6, 56.3, and 22.5 by ZnO/Zn–Cr HACs, P25 and ZnO, respectively. Compared with ZnO and P25, the ZnO/Zn–Cr HACs showed comparable decolorization ability towards CR dye.

The possible mechanism of CR decolorization by ZnO/Zn–Cr HACs

Based on the above results, the probable mechanism for the decolorization of CR

electrons in CrO_6 octahedron under visible light irradiation could play a crucial role in the photodegradation of dye solution by Zn–Cr HACs (Eq. 9) [42]. The charge transfer spectra from oxygen atoms of the lattice to the Cr^{+3} ions in ZnO/Zn–Cr HACs led to a more efficient charge separation with the creation of electrons and holes [43], after which the migrated e^- reacted with the oxygen molecule (O_2) that dissolved in aqueous solution to yield $O_2^{\cdot-}$ (Eq. 10). At the same time VB holes of ZnO react with water to produce highly reactive hydroxyl ($\cdot$OH) radical (Eq. 11) [44]. The superoxide radical anion and hydroxyl radical could be also utilized to degrade further CR molecules to all types of inorganic small molecular such as CO_2, H_2O and other small molecule by products (Eq. 12).

$$CR \text{ (in aqueous solution)} + ZnO/Zn-Cr \text{ HACs}$$
$$\rightarrow CR^* - ZnO + \ CR^* - Zn - Cr \text{ HACs} \tag{7}$$

$$CR^* - ZnO + hv \rightarrow CR^* - ZnO\left(e_{CB}^- + h_{VB}^+\right) \tag{8}$$

$$ZnCr - LDH + hv \rightarrow CR^* - ZnCr - LDH \ \left(e_{CB}^- + h_{VB}^+\right) \tag{9}$$

$$e_{CB}^- + O_2 \rightarrow O_2^{\cdot-} \tag{10}$$

$$h_{VB}^+ + H_2O \rightarrow \dot{\ }OH + H^+ \tag{11}$$

$$CR + h_{VB}^+/\dot{\ }OH/O_2^{\cdot-} \rightarrow\rightarrow CO_2 + H_2O + \text{other small molecule byproducts} \tag{12}$$

Conclusions

The present study shows that ZnO/Zn–Cr HACs is a potential and reusable material for the effective removal of dye from aqueous solution. The maximum adsorption capacity of ZnO/Zn–Cr HACs can be as high as 426 mg g^{-1} for CR dye at room temperature. The ZnO/Zn–Cr HACs had an excellent capacity for CR with an adsorption efficiency of 99 %. The adsorption kinetics and the adsorption isotherm of ZnO/Zn–Cr HACs were in good agreement with the pseudo-second-order model and the Langmuir model, respectively, which indicates that the rate-limiting step was chemisorption and adsorption sites were homogeneous. In addition, ZnO/Zn–Cr HACs retained its activity after several recycles for the CR photocolorization. Compared with ZnO and P25, the ZnO/Zn–Cr HACs showed comparable photocatalytic ability towards CR dye. Therefore, it is expected that the ZnO/Zn–Cr HACs with hierarchical structure and high specific surface areas in this work can be potentially used as an effective and reusable environmentally friendly materials for the effective removal of pollutants in wastewater treatment.

References

1. Y. Tang, G. Zhang, C. Liu, S. Luo, X. Xu, L. Chen, B. Wang, J. Hazard. Mater. **252–253**, 115 (2013)
2. J.L. Wang, L.J. Xu, Crit. Rev. Env. Sci. Technol. **42**, 251 (2012)
3. M.A. Shannon, W.B. Paul, M. Elimelech, J.G. Georgiadis, B.J. Marinas, A.M. Mayes, Nature **452**, 301 (2008)
4. A. Faki, M. Turan, O. Ozdemir, A.Z. Turan, Ind. Eng. Chem. Res. **47**, 6999 (2008)
5. Z. Aksu, Process Biochem. **40**, 997 (2005)
6. S.B. Wang, H.Q. Sun, H.M. Ang, M.O. Tadé, Chem. Eng. J. **226**, 336 (2013)
7. X. Zhuang, Y. Wan, C. Feng, Y. Shen, D. Zhao, Chem. Mater. **21**, 706 (2009)
8. C. Cao, L. Xia, C. Chen, X. Shi, Q. Cao, L. Gao, Powder Technol. **260**, 90 (2014)
9. G. Crin, Bioresour. Technol. **97**, 1061 (2006)
10. V.K. Gupta, P.J.M. Carrott, M.M.L. Ribeiro Carrott, Suhas, Crit. Rev. Env. Sci. Technol. **39**, 783 (2009)
11. H. Zhang, H. Fu, D. Zhang, J. Hazard. Mater. **172**, 654 (2009)
12. A. Phuruangrat, S. Mad-ahin, O. Yayapao, S. Thongtem, T. Thongtem, Res. Chem. Intermed. (2015). doi:10.1007/s11164-015-1963-z
13. H.Y. Zhu, Y.Q. Fu, R. Jiang, J. Yao, L. Liu, Y.W. Chen, L. Xiao, G.M. Zeng, Appl. Surf. Sci. **285**, 865 (2013)
14. D. Bi, Y. Xu, Langmuir **27**, 9359 (2011)
15. C.Y. Chen, J.C. Chang, A.H. Chen, J. Hazard. Mater. **185**, 430 (2011)
16. H. Zhu, R. Jiang, Y. Fu, Y. Guan, J. Yao, L. Xiao, G. Zeng, Desalination **286**, 41 (2012)
17. N. Baliarsingh, K.M. Parida, G.C. Pradhan, Ind. Eng. Chem. Res. **53**, 3834 (2014)
18. M. Lan, G. Fan, L. Yang, F. Li, Ind. Eng. Chem. Res. **53**, 12943 (2013)
19. M. Sarkarat, S. Komarneni, Z. Rezvani, X. Wu, S. Yin, T. Sato, Z.F. Yan, Appl. Clay Sci. **80–81**, 390 (2013)
20. M. Shao, J. Han, M. Wei, D.G. Evans, X. Duan, Chem. Eng. J. **168**, 519 (2011)
21. X. Cheng, X. Huang, X. Wang, B. Zhao, A. Chen, D. Sun, J. Hazard. Mater. **169**, 958 (2009)
22. J. Zhou, S. Yang, J. Yu, Z. Shu, J. Hazard. Mater. **192**, 1114 (2011)
23. A.R. Auxilio, P.C. Andrews, P.C. Junk, L. Spiccia, D. Neumann, W. Raverty, N. Vanderhoek, Polyhedron **26**, 3479 (2007)
24. N.K. Lazaridis, T.D. Karapantsios, D. Georgantas, Water Res. **37**, 3023 (2003)
25. K. Morimoto, K. Tamura, N. Iyi, J. Ye, H. Yamada, J. Phys. Chem. Solids **72**, 1037 (2011)
26. K.H. Goh, T.T. Lim, Z. Dong, Water Res. **42**, 1343 (2008)
27. D. Mohan, C.U. Pittman, J. Hazard. Mater. **142**, 1 (2007)
28. R. Rojas, C. Barriga, C.P. De Pauli, M.J. Avena, Mater. Chem. Phys. **119**, 303 (2010)
29. Z. Zhang, C. Shao, X. Li, L. Zhang, H. Xue, C. Wang, Y. Liu, J. Phy. Chem. C **114**, 7920 (2010)
30. J.K. Vaishnav, S.S. Arbuj, S.B. Rane, D.P. Amalnerkar, RSC Adv. **4**, 47637 (2014)
31. P.S. Badgujar, S.S. Arbuj, J.M. Mali, S.B. Rane, U.P. Mulik, J. Nanoeng. Nanomanuf. **4**, 65 (2014)
32. K. Dutta, S. Das, A. Pramanik, J. Colloid Interface Sci. **366**, 28 (2012)
33. S. Yuan, Y. Li, Q. Zhang, H. Wang, Colloids Surf. A **348**, 76 (2009)
34. W. Wang, P. Serp, P. Kalck, J.L. Faria, J. Mol. Catal. A. **235**, 194 (2005)
35. G. Bayramoglu, B. Altintas, M.Y. Arica, Chem. Eng. J. **152**, 339 (2009)
36. A. Özcan, E.M. Öncü, A.S. Özcan, J. Hazard. Mater. **B129**, 244 (2006)
37. J. Wang, R.H. Li, Z.H. Zhang, W. Sun, R. Xu, Y.P. Xie, Z.Q. Xing, X.D. Zhang, Appl. Catal. A **334**, 227 (2008)
38. H. Zhu, R. Jiang, L. Xiao, Y. Chang, Y. Guan, X. Li, G. Zeng, J. Hazard. Mater. **169**, 933 (2009)
39. L. Zhang, F. Li, D.G. Evans, X. Duan, Mater. Chem. Phys. **87**, 402 (2004)
40. H. Liu, Q. Jiao, Y. Zhao, H. Li, C. Sun, X. Li, J. Alloys Compd. **496**, 317 (2010)
41. B. Subash, B. Krishnakumar, M. Swaminathan, M. Shanthi, Langmuir **29**, 939 (2013)
42. M. Lan, G. Fan, L. Yang, F. Li, Ind. Eng. Chem. Res. **53**, 12943 (2014)
43. L. Mohapatra, K.M. Parida, Sep. Purif. Technol. **91**, 73 (2012)
44. R. Velmurugan, M. Swaminathan, Sol. Energy Mater. Sol. Cells **95**, 942 (2011)